

000 001 002 003 004 005 006 007 008 009 010 011 012 013 014 015 016 017 018 019 020 021 022 023 024 025 026 027 028 029 030 031 032 033 034 035 036 037 038 039 040 041 042 043 044 045 046 047 048 049 050 051 052 053 DYMixOP: GUIDING NEURAL OPERATOR DESIGN FOR PDES FROM A COMPLEX DYNAMICS PERSPEC- TIVE WITH LOCAL-GLOBAL-MIXING

006
007 **Anonymous authors**
008 Paper under double-blind review

011 ABSTRACT

013 A primary challenge in using neural networks to approximate nonlinear dynamical
014 systems governed by partial differential equations (PDEs) is transforming these
015 systems into a suitable format, especially when dealing with non-linearizable dy-
016 namics or the need for infinite-dimensional spaces for linearization. This paper
017 introduces DyMixOp, a novel neural operator framework for PDEs that integrates
018 insights from complex dynamical systems to address this challenge. Grounded
019 in inertial manifold theory, DyMixOp transforms infinite-dimensional nonlinear
020 PDE dynamics into a finite-dimensional latent space, establishing a structured
021 foundation that maintains essential nonlinear interactions and enhances physical
022 interpretability. A key innovation is the Local-Global-Mixing (LGM) transfor-
023 mation, inspired by convection dynamics in turbulence. This transformation effec-
024 tively captures both fine-scale details and nonlinear interactions, while mitigating
025 spectral bias commonly found in existing neural operators. The framework is
026 further strengthened by a dynamics-informed architecture that connects multiple
027 LGM layers to approximate linear and nonlinear dynamics, reflecting the temporal
028 evolution of dynamical systems. Experimental results across diverse PDE bench-
029 marks demonstrate that DyMixOp achieves state-of-the-art performance, signifi-
030 cantly reducing prediction errors, particularly in convection-dominated scenarios
031 reaching up to 86.7%, while maintaining computational efficiency and scalability.

032 1 INTRODUCTION

033 Partial differential equations (PDEs) are the mathematical backbone for describing chaotic behav-
034 iors and understanding underlying mechanics in dynamical systems. They are distributed in various
035 fields including climate (Bi et al., 2023; Lam et al., 2023), molecular dynamics (Rapaport, 2004),
036 ecological modeling (Blasius et al., 1999), brain activity (Breakspear, 2017), chemistry (Jensen,
037 2017), heat transfer (Howell et al., 2020) and turbulent flows (Mukherjee et al., 2023). Predicting
038 the dynamics of complex systems by solving PDEs is crucial for scientific and engineering applica-
039 tions. As a result, a variety of numerical methods have been developed (Dennis Jr & Schnabel, 1996;
040 Moin & Mahesh, 1998), including the finite difference method (Smith, 1985), finite volume method
041 (Versteeg, 2007), lattice Boltzmann method (Succi, 2001) and finite element method (Zienkiewicz,
042 1971). Despite the high fidelity of simulations produced by traditional approaches, they become in-
043 efficient with frequent recalculations whenever initial conditions or equation parameters are altered.

044 In recent years, data-driven methods have thrived across various disciplines (Jordan & Mitchell,
045 2015). Among these approaches, neural networks have garnered significant attention from re-
046 searchers due to their excellent performance in other fields such as large language modeling (Bah-
047 danau, 2014), image recognition (Simonyan & Zisserman, 2014) and games (Mnih et al., 2015;
048 Vinyals et al., 2019). Therefore they are perceived as promising tools to overcome the limitations of
049 traditional methods and offer more possibilities for solving ill-defined problems. In terms of the ap-
050 proximation way whether the transformation of the neural layer spans the entire input domain, they
051 can be roughly classified into four kinds: **the local transformation**, **the global transformation**,
052 **the local-global adding transformation (LGA)**, **the local-local mixing transformation (LLM)**.
053 Due to the complete architecture complexity of neural networks, here we only focus on the single

054 neural layer. The general transformation of a neural layer can be defined in the form of
 055

$$(G_\theta v)(x) = \int_{D_\tau} g_\theta(x, \tau) v(\tau) d\tau, \quad x \in D_x \quad (1)$$

056 where G_θ is a integral transformation parameterized by parameter sets $\theta \in \Theta$ in neural networks,
 057 g_θ represents a integral kernel function parameterized by neural networks, D_τ and D_x are bounded
 058 domains in \mathbb{R}^d ($d \in \mathbb{Z}$ denotes the spatial dimension), $\tau \in D_\tau$ and $x \in D_x$ are variables in the input
 059 and output domains respectively, and v is defined on D_τ . When D_τ is the partial domain $P_\tau \subset \mathbb{R}^d$, it
 060 is the local transformation. When D_τ is the entire domain $E_\tau \subset \mathbb{R}^d$, it is the global transformation.
 061 Mixing here means the element-wise product and adding means the element-wise addition between
 062 transformations.
 063

064 2 RELATED WORK

065 **Models with Local Transformations.** In the 1990s, Lagaris et al. (1998) trained a shallow FCNN to
 066 solve PDEs. With the recent revival of deep learning (LeCun et al., 2015), Raissi et al. (2019) developed
 067 this idea based on modern techniques of deep learning and proposed physics-informed neural
 068 networks (PINNs) to solve PDEs. Many efforts have been made to develop PINNs (Pang et al.,
 069 2019; Lu et al., 2021b; Karniadakis et al., 2021). To avoid unaffordable computational cost, all of
 070 the above studies limited input to only a few points at once and thus are the local transformation.
 071 To address the curse of dimensionality in image inputs, plenty of works were performed to approximate
 072 the evolution operator using CNNs (Qu et al., 2022; Gao et al., 2021; List et al., 2022). Some
 073 convolutional neural layer-based network architectures were also developed to solve PDE problems,
 074 including generative adversarial networks for two-dimensional turbulence (Kim et al., 2024; 2021),
 075 and autoencoder for three-dimensional turbulence (Xuan & Shen, 2023). Obviously, these convolutional
 076 neural layer-based network architectures fall into the scope of the local transformation.
 077

078 **Models with Global Transformations.** The self-attention blocks in Transformers model using
 079 the composite matricial local-local mixing transformations belong to the global transformation
 080 (Vaswani, 2017), and how the kernel function can be extended to the vanilla transformer formula
 081 is detailed in (Kovachki et al., 2023). Some researches were performed to construct a transformer-
 082 based framework to solve PDE problems (Cao, 2021; Li et al., 2022).
 083

084 **Models with LLM Transformations.** More complex neural network architectures targeted at LLM
 085 convolutional transformations for a more powerful nonlinear representation. Shi et al. (2015) combined
 086 convolutional transformations with the classical long short-term memory networks (LSTMs),
 087 where the cell state and latent state of LSTMs are obtained from element-wise products. Long
 088 et al. (2018) combined the traditional numerical schemes with the LLM convolutional transformation
 089 to solve PDEs problems. Similarly, Rao et al. (2023) also developed a framework to encode
 090 the physics and numerical schemes based on LLM convolutional transformation. However, the local
 091 convolutional transformation heavily depends on mesh discretization, typically leading to a degraded
 092 performance under changes in mesh discretization.
 093

094 **Models with LGA Transformations.** To address mesh dependency in local convolutional trans-
 095 formations, two approaches exist: constructing networks with mesh-independent discrete methods,
 096 such as one-size convolutional kernels, or approximating the kernel in an auxiliary space. The graph
 097 kernel network framework approximates the kernel in graph space using local convolutional and
 098 graph transformations (Li et al., 2020b). To incorporate global information and improve efficiency,
 099 spectral methods were introduced, representing complex patterns compactly (Trefethen, 2000). Li
 100 et al. (2020a) developed the Fourier neural operator, replacing graph approximations with Fourier
 101 layers to process entire domains. This inspired other spectral-based operators to transform kernels
 102 into spectral spaces, such as wavelet (Tripura & Chakraborty, 2022) and Laplace neural operators
 103 (Cao et al., 2024).
 104

105 **Other Models.** It is worth mentioning that due to the variety of network variants and high-level
 106 defined architectures, it is sometimes hard to directly classify their transformation. For example,
 107 the concept of the neural operator was also presented by Lu et al. (2021a). . They developed the
 108 DeepONet framework composed of the trunk network and branch network but transformations are
 109 not explicitly defined.
 110

108

3 CHALLENGES AND METHODOLOGIES

109

110

Operator Definition. In this work, we focus on the form of neural operators due to their mesh
111 independence and generalization to unseen parameters. Here, we first outline the concept of operator
112 approximation. Given a spatial domain $D \subset \mathbb{R}^d$ with a spatial dimension d , an operator mapping
113 from the input space to the solution space is defined as:

114
$$\mathcal{G} : \mathcal{I}(D; \mathbb{R}^{d_i}) \rightarrow \mathcal{U}(D; \mathbb{R}^{d_u}), \quad (2)$$
115

116 where $\mathcal{I}(D; \mathbb{R}^{d_i})$ and $\mathcal{U}(D; \mathbb{R}^{d_u})$ are Banach spaces representing the input and solution spaces,
117 respectively, and $d_i, d_u \in \mathbb{N}$ denote their corresponding dimensions. Specifically, it often involves
118 the evolution of the system in the context of PDEs and thus considers \mathcal{G} an evolutionary operator.

119

Challenges in Nonlinear Dynamical System Approximation. To design a neural evolution operator
120 that can effectively approximate autonomous dynamical systems, we first need to understand
121 the intrinsic connection between the original dynamical system and the dynamics expressed within
122 the neural network framework. This theoretical foundation is crucial for guiding us on how to sim-
123 plify the infinite-dimensional partial differential equation dynamics into a finite-dimensional and
124 expressive latent dynamics. The general form of an autonomous dynamical system is:

125
$$\frac{\partial u(t)}{\partial t} = F(u), \quad t \in [0, T] \quad (3)$$
126

127 where $u \in \mathcal{U}(D; \mathbb{R}^{d_u})$ is a solution of dynamical systems, and $F : \mathcal{U}(D; \mathbb{R}^{d_u}) \rightarrow \mathcal{U}(D; \mathbb{R}^{d_u})$
128 is an operator that acts on the solution u at each time t and represents the dynamics of u . The
129 operator F may consist of linear operators, nonlinear operators, and source terms, depending on the
130 specific dynamical system being modeled. Generally, nonlinear dynamical systems are addressed
131 by transforming the system into a (partially) linearized form or mapping it to a new representation
132 suitable for analysis and control utilizing a dimension-shifting operator \mathcal{T} . After applying $\mathcal{T} : \mathcal{U}(D; \mathbb{R}^{d_u}) \rightarrow \mathcal{V}(D; \mathbb{R}^{d_v})$, the solution u is transformed to a latent state $v = \mathcal{T}(u)$ in a latent space
133 $\mathcal{V}(D; \mathbb{R}^{d_v})$, with its latent dynamics given by:

134
$$\frac{\partial v(t)}{\partial t} = \tilde{F}(v), \quad t \in [0, T] \quad (4)$$
135

136 where $\tilde{F} : \mathcal{V}(D; \mathbb{R}^{d_v}) \rightarrow \mathcal{V}(D; \mathbb{R}^{d_v})$ is an operator that acts on v and represents the dynamics
137 of v . Unfortunately, for known dynamical systems, the operator \mathcal{T} is difficult to determine; for
138 unknown dynamical systems, even $F(u)$ remains unresolved. These difficulties pose significant
139 challenges for solving arbitrary complex dynamical systems. Hopefully, machine learning methods
140 can approximate them in aid of data alone but often implicitly assume locally linearized dynamical
141 systems or globally linearizable nonlinear systems (Cenedese et al., 2022).

142 However, under this simplified assumption, two major challenges arise: (i) achieving linearization
143 for nonlinear systems often requires an infinite-dimensional latent space \mathcal{V} (Brunton et al., 2022),
144 i.e. $d_v \rightarrow \infty$, making direct computation impossible, and (ii) some dynamical systems may possess
145 intrinsically non-linearizable dynamics, meaning \tilde{F} retains nonlinear components even in an infinite-
146 dimensional \mathcal{V} (Cenedese et al., 2022).

147

Inertial Manifold Theory for Dimensional Reduction. Fortunately, inertial manifold theory
148 (Foias et al., 1988) provides a rigorous framework for (i) reducing such systems to finite-dimensional
149 dynamics that capture the essential long-term behavior and (ii) remaining necessary nonlinearity.
150 This approach offers a principled foundation for developing physically interpretable models.

151 An inertial manifold \mathcal{M} is a finite-dimensional, Lipschitz continuous manifold embedded within a
152 Hilbert space \mathcal{H} . Any state $v \in \mathcal{M}$ can be uniquely decomposed into a low-mode component \hat{v} and
153 a high-mode component that is a function of the low-mode one $v = \hat{v} + \Phi(\hat{v})$. Here, $\hat{v} = \mathcal{P}_m v$ is
154 the projection of v onto the first d_m eigenmodes, and Φ is a Lipschitz continuous function mapping
155 the low modes to the corresponding high modes in the orthogonal complement space.

156 Consider latent dynamics governed by $\frac{\partial v}{\partial t} = \mathcal{L}(v) + \mathcal{N}(v)$, where \mathcal{L} and \mathcal{N} are linear and nonlinear
157 operators, respectively. If the long-term dynamics are confined to an inertial manifold \mathcal{M} , we can
158 project the governing equations onto the low-mode space $\mathcal{V}_r = \mathcal{P}_m \mathcal{V}$. Substituting $v = \hat{v} + \Phi(\hat{v})$
159 into the dynamics and applying the projection \mathcal{P}_m yields the exact reduced dynamics for \hat{v} :

160
$$\frac{\partial \hat{v}}{\partial t} = \mathcal{P}_m \mathcal{L}(\hat{v} + \Phi(\hat{v})) + \mathcal{P}_m \mathcal{N}(\hat{v} + \Phi(\hat{v}))$$

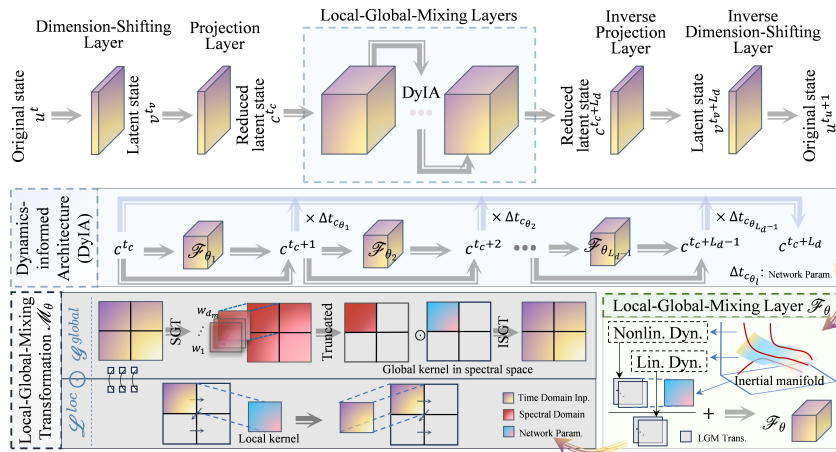


Figure 1: Illustration of the DyMixOp model composed of the dimension-shifting layer and its inverse, the projection layer and its inverse, and the LGM layers that adopt LGM transformations to approximate dynamics within the dynamics-informed architecture.

Under the common assumption that the nonlinear interactions involving the slave high modes $\Phi(\hat{v})$ can be modeled as a correction term, we can approximate the above as:

$$\frac{\partial \hat{v}}{\partial t} \approx \mathcal{L}\hat{v} + \mathcal{P}_m\mathcal{N}(\hat{v}) + \mathcal{P}_m\mathcal{R}[\mathcal{N}(\hat{v})] \quad (5)$$

where \mathcal{R} is a residual operator capturing the influence of the high-mode interactions. This derivation offers a clear blueprint for constructing a reduced-order model and motivates the following design principle of our neural operator by translating the latent state \hat{v} into the spectral coefficients c (further derivation under additional assumptions see the Appendix).

Proposition 1. (Principled Architectural Design) Our proposed neural operator, \mathcal{G}^\dagger , is constructed as a direct functional analogue of the reduced dynamics dictated by inertial manifold theory. By projecting Equation 5 onto a spectral basis to obtain dynamics for the reduced latent state c (by acting \mathcal{P}_m on v), the network is designed to approximate the evolution operator $\mathcal{F}(c)$ where

$$\frac{\partial c(t)}{\partial t} = \mathcal{F}(c) \approx \mathcal{L}_c c + \mathcal{A}[\mathcal{N}_c(c)] \quad (6)$$

Specifically, the architecture \mathcal{G}^\dagger is structured to explicitly model the components of $\mathcal{F}(c)$: (i) a linear component approximates the linear operator $\mathcal{L}_c : \mathcal{C}(D; \mathbb{R}^{d_m}) \rightarrow \mathcal{C}(D; \mathbb{R}^{d_m})$, and (ii) a nonlinear component approximates the operator $\mathcal{A}[\mathcal{N}_c(\cdot)]$, where $\mathcal{N}_c : \mathcal{C}(D; \mathbb{R}^{d_m}) \rightarrow \mathcal{C}(D; \mathbb{R}^{d_m})$ is a nonlinear operator, $\mathcal{A} : \mathcal{C}(D; \mathbb{R}^{d_m}) \rightarrow \mathcal{C}(D; \mathbb{R}^{d_m})$ is an operator mapping the low-mode component to the full-mode component.

This proposition formalizes the link between theory and method. Instead of being merely inspired by the theory, our network architecture is a direct implementation of the mathematical structure that the theory predicts. This provides a principled foundation for designing neural layers that approximate arbitrary complex dynamics with enhanced physical interpretability and generalization capabilities.

Local-Global-Mixing Transformation. Inspired by the profound impact of complex physical systems on network design (Ho et al., 2020; Chen et al., 2018), particularly the multi-scale dynamics of turbulence and the role of its convection term, we sought to create a transformation capable of capturing similarly intricate dynamics. The convection term, defined by the product of a variable c and its gradient $\frac{\partial c}{\partial x}$, naturally embodies a form of local-global interaction. The variable c itself is intrinsically localized, tied to its specific spatial position, suggesting the behavior of a local operation like convolution. In contrast, the computation of its gradient $\frac{\partial c}{\partial x}$ relies on information from the wider domain, often requiring global approaches such as spectral methods. This inherent structure within the convection term, where local state mixes with global gradient information, provides the core inspiration for our novel LGM transformation. This architecture is designed to explicitly combine the benefits of local and spectral global transformations, mirroring the essential mixing process

observed in convection to handle complex multi-scale features and mitigating the spectral bias in existing neural operators, as follows:

Definition 1. (Local-Global-Mixing Transformation) The Local-Global-Mixing (LGM) transformation is defined as a parameterized operator that combines localized and global information from the input state c in an element-wise multiplicative form. Specifically, it is given by:

$$\mathcal{M}_\theta(c) = \mathcal{L}_\theta^{loc}(c) \odot \mathcal{G}_\theta^{glob}(c) = \left(\int_{P_\tau} p_\theta(x, \tau) c(\tau) d\tau \right) \odot \left(\int_{E_\tau} e_\theta(x, \tau) c(\tau) d\tau \right), \quad (7)$$

where \mathcal{L}_θ^{loc} is the local integral operator, $\mathcal{G}_\theta^{glob}$ is the global integral operator, c is the reduced latent state. $p_\theta(x, \tau) : D_x \times P_\tau \rightarrow \mathbb{R}$ is the local kernel function, responsible for capturing fine-grained, position-specific interactions. $e_\theta(x, \tau) : D_x \times E_\tau \rightarrow \mathbb{R}$ is the global kernel function, designed to incorporate domain-wide information and relationships. They are parameterized by a set of parameters θ . P_τ and E_τ are integration domains corresponding to local and global interactions, respectively. \odot denotes the element-wise (Hadamard) product.

The transformation provides a versatile way to represent both linear and nonlinear dynamics. (i) For linear dynamics, setting $p_\theta(x, \tau) = \frac{1}{P_\tau c}$ or $e_\theta(x, \tau) = \frac{1}{E_\tau c}$ makes \mathcal{M}_θ a linear integral operator. (ii) For nonlinear dynamics, parameterized kernels $p_\theta(x, \tau)$ and $e_\theta(x, \tau)$ turn \mathcal{M}_θ into a nonlinear operator. This flexibility allows the LGM transformation to model both types effectively, offering a unified approach for complex dynamical systems.

Local-Global-Mixing Layers. Due to the flexibility of the LGM transformation in representing both linear and nonlinear dynamics, we employ two separate LGM transformations to approximate the linear component \mathcal{L}_c and the nonlinear component \mathcal{N}_c in the above design principle, with the reduced latent state as input.

\mathcal{A} primarily involves high-mode small quantities that emphasize local interactions. So we can use a local transformation to approximate the operator \mathcal{A} , facilitating the complexity of neural layers, as follows:

$$\mathcal{F}_\theta(c) = \mathcal{M}_\theta^{\mathcal{L}}(c) + \mathcal{H}_\theta \circ \mathcal{M}_\theta^{\mathcal{N}}(c), \quad (8)$$

where $\mathcal{M}_\theta^{\mathcal{L}} : \mathcal{C}(D; \mathbb{R}^{d_m}) \rightarrow \mathcal{C}(D; \mathbb{R}^{d_m})$, $\mathcal{M}_\theta^{\mathcal{N}} : \mathcal{C}(D; \mathbb{R}^{d_m}) \rightarrow \mathcal{C}(D; \mathbb{R}^{d_m})$ indicate LGM transformations approximating the linear dynamics $\mathcal{L}_c c$ and the nonlinear dynamics $\mathcal{N}_c(c)$, respectively, and $\mathcal{H}_\theta : \mathcal{C}(D; \mathbb{R}^{d_m}) \rightarrow \mathcal{C}(D; \mathbb{R}^{d_m})$ the local transformation. Sometimes dynamical systems may involve composite operators, such as two higher-order derivatives in the Kuramoto-Sivashinsky system, and one can utilize more transformations to finely approximate different components in operators. Finally, we can construct a LGM layer, which considers the reduced latent state c as input, to represent the reduced latent dynamics with the definition as follows:

Definition 2. (Reduced Latent Dynamics Represented by Single LGM Layer) The reduced latent dynamics represented by a single Local-Global-Mixing (LGM) neural layer is a sum of a local transformation \mathcal{H}_θ and multiple LGM transformations \mathcal{M}_θ , each capturing distinct components or scales of the system's behavior. Specifically, the dynamics are formulated as:

$$\mathcal{F}_\theta(c) = \sum_{a=1}^{n_l} \mathcal{M}_\theta^{\mathcal{L}^a}(c) + \mathcal{H}_\theta \left[\sum_{b=1}^{n_n} \mathcal{M}_\theta^{\mathcal{N}^b}(c) \right], \quad (9)$$

where n_l, n_n are the numbers of the linear and nonlinear LGM transformation, respectively, and c is the reduced latent state.

Dynamics-Informed Architecture. In deep learning, enhancing the representational capacity of neural networks is often achieved by stacking multiple layers. To integrate this concept into the DyMixOp framework, an architecture designed for connecting LGM layers is proposed based on the evolution of dynamics. By introducing time transformations between each dynamics and learnable evolutionary step (derivation see Appendix), we can get the following formula of the output:

$$c_{L_d} = c_0 + \sum_{l=1}^{L_d} \Delta t_{c_{\theta_l}} \mathcal{F}_{\theta_l}(c_{l-1}) \quad (10)$$

270 where $\Delta t_{c_{\theta_l}}$ is a parameterized evolutionary step and the input to each layer c_{l-1} is recursively
 271 defined as $c_{l-1} = c_{l-2} + \mathcal{F}_{\theta_{l-1}}(c_{l-2}), l = 2, \dots, L_d$.
 272

273 **DyMixOp.** Here we can assemble the above components to propose a novel neural operator named
 274 DyMixOp shown in Fig. 1. For clarity, let us assume $k = 0$ and then denote the temporal input
 275 sequence $[u^{t_{i-k}}, \dots, u^{t_i}]$ by u^t . Given a depth $L_d \in \mathbb{N}$, the DyMixOp takes the following composite
 276 form:
 277

$$\mathcal{G}^\dagger(u^t; \theta) = \mathcal{T}^{-1} \circ \mathcal{P}_m^{-1} \circ \mathcal{C} \circ \mathcal{P}_m \circ \mathcal{T}(u^t), \quad (11)$$

278 where $\mathcal{T} : \mathcal{U}(D; \mathbb{R}^{d_u}) \rightarrow \mathcal{V}(D; \mathbb{R}^{d_v})$ is a neural operator (or neural layer in the context of neural
 279 network) that shifts the channel dimension, transforming the original state u^t into the latent state v^t ,
 280 $\mathcal{P}_m : \mathcal{V}(D; \mathbb{R}^{d_v}) \rightarrow \mathcal{C}(D; \mathbb{R}^{d_m})$ is a neural operator that projects state onto a low-dimensional
 281 space, transforming the latent state v^t into the reduced latent state c^t . $\mathcal{T}^{-1} : \mathcal{V}(D; \mathbb{R}^{d_v}) \rightarrow$
 282 $\mathcal{U}(D; \mathbb{R}^{d_u})$ and $\mathcal{P}_m^{-1} : \mathcal{C}(D; \mathbb{R}^{d_m}) \rightarrow \mathcal{V}(D; \mathbb{R}^{d_v})$ are neural operators that reverse the transfor-
 283 mations of \mathcal{T} and \mathcal{P}_m , respectively.
 284

285 At the heart of the DyMixOp is the composite nonlinear operator $\mathcal{C} : \mathcal{C}(D; \mathbb{R}^{d_m}) \rightarrow \mathcal{C}(D; \mathbb{R}^{d_m})$.
 286 This comprises L_d LGM layers that are integrated within a dynamics-informed network architecture,
 287 and are expressed as follows:
 288

$$\mathcal{C}(c) = c_0 + \sum_{l=1}^{L_d} \Delta t_{c_{\theta_l}} \mathcal{F}_{\theta_l}(c_{l-1}), \quad (12)$$

290 where $\Delta t_{c_{\theta_l}}$ is a parameterized evolutionary step and the input c_{l-1} to each layer is recursively
 291 defined as $c_{l-1} = \sigma(c_{l-2} + \mathcal{F}_{\theta_{l-1}}(c_{l-2})), l = 2, \dots, L_d$, where $\sigma : \mathbb{R}^{d_m} \rightarrow \mathbb{R}^{d_m}$ is a nonlinear
 292 activation function applied element-wise, and the LGM layer \mathcal{F}_{θ_l} is defined as
 293

$$\mathcal{F}_{\theta}(c) = \sum_{a=1}^{n_l} \mathcal{M}_{\theta}^{\mathcal{L}^a}(c) + \mathcal{H}_{\theta} \left[\sum_{b=1}^{n_n} \mathcal{M}_{\theta}^{\mathcal{N}^b}(c) \right], \quad (13)$$

294 where $\mathcal{M}_{\theta}^{\mathcal{N}^b} : \mathcal{C}(D; \mathbb{R}^{d_m}) \rightarrow \mathcal{C}(D; \mathbb{R}^{d_m})$ and $\mathcal{M}_{\theta}^{\mathcal{L}^a} : \mathcal{C}(D; \mathbb{R}^{d_m}) \rightarrow \mathcal{C}(D; \mathbb{R}^{d_m})$ are nonlinear
 295 and linear LGM transformations, respectively, n_n, n_l are the number of nonlinear and linear LGM
 296 transformations, respectively, and $\mathcal{H}_{\theta} : \mathcal{C}(D; \mathbb{R}^{d_m}) \rightarrow \mathcal{C}(D; \mathbb{R}^{d_m})$ is the local transformation. The
 297 nonlinear LGM transformation $\mathcal{M}_{\theta}^{\mathcal{N}}$ is defined as
 298

$$(\mathcal{M}_{\theta}^{\mathcal{N}} c)(x) = (\mathcal{L}_{\theta}^{\text{loc}} c)(x) \odot (\mathcal{G}_{\theta}^{\text{glob}} c)(x), \quad (14)$$

301 where $(\mathcal{L}_{\theta}^{\text{loc}} c)(x) = \int_{P_{\tau}} p_{\theta}(x, y) c(y) dy$ and $(\mathcal{G}_{\theta}^{\text{glob}} c)(x) = \int_{E_{\tau}} e_{\theta}(x, y) c(y) dy$ are the local trans-
 302 formation and the global transformation, respectively, where $p_{\theta} : D \times P_{\tau} \rightarrow \mathbb{R}$ and $e_{\theta} : D \times E_{\tau} \rightarrow \mathbb{R}$
 303 are kernel functions parameterized by θ , and the integrals are well-defined over the domain P_{τ} and
 304 E_{τ} , \odot denotes the element-wise (Hadamard) product. The definition of linear operator $\mathcal{M}_{\theta}^{\mathcal{L}}$ is
 305 similar to the nonlinear one, but the global transformation or local transformation is specified as
 306 an indicator function $\mathbf{1}_D(x)$ depending on cases. Consequently, this formulation ensures that the
 307 DyMixOp captures both linear and nonlinear dynamics through local and global dependencies.
 308

309 **Detailed Implementation for DyMixOp.** This work adopts key empirical insights from ML: local
 310 convolutions often outperform global spectral transforms, and applying activation functions to out-
 311 puts typically boosts network performance. Accordingly, the global kernel e_{θ} in $\mathcal{M}_{\theta}^{\mathcal{L}^a}$ is fixed as
 312 $\frac{1}{E_{\tau} c}$, effectively reducing it to an indicator function $\mathbf{1}_D(x)$. Activations are applied at each interme-
 313 diate state c_{l-1} . In the inertial manifold framework, \mathcal{T} ideally maps to infinite dimensions but is
 314 practically set to twice the dimension of \mathcal{P}_m , whose optimal size remains a tunable hidden hyper-
 315 parameter. For efficiency, \mathcal{T} , \mathcal{P}_m , and their inverses are implemented as local transforms—though
 316 this is flexible per use case. All transformations— \mathcal{T} , \mathcal{P}_m , their inverses, \mathcal{H}_{θ} , and local compo-
 317 nents of $\mathcal{M}_{\theta}^{\mathcal{L}^a}$ and $\mathcal{M}_{\theta}^{\mathcal{N}^b}$ —use 1×1 convolutions to ensure mesh-invariance. Global components
 318 in $\mathcal{M}_{\theta}^{\mathcal{N}^b}$ employ trainable truncated Fourier transforms, following FNO. For performance-critical
 319 tasks, larger convolutional kernels may be used— 1×1 is not mandatory.
 320

321 **Operator Approximation.** Computationally, the operator \mathcal{G} must be discretized on the physical
 322 space and time. Given a discrete time sequence $\{t_i\}_{i=0}^T$ and states $u^{t_i}, u^{t_{i+1}} \in \mathcal{U}(D; \mathbb{R}^{d_u})$, sampled
 323 from a probability distribution P_u over $\mathcal{U}(D; \mathbb{R}^{d_u})$, their relationship is defined as $u^{t_{i+1}} = \mathcal{G}(u^{t_i})$

324 for $i = 0, 1, \dots, T - 1$. The objective is to approximate the operator \mathcal{G} using the DyMixOp model
 325 parameterized by $\theta \in \Theta$, where Θ denotes the parameter space with dimensionality determined
 326 by the chosen architecture. Thus, the approximation of \mathcal{G} using the DyMixOp is formulated as the
 327 following optimization problem:

$$328 \min_{\theta \in \Theta} \mathbb{E}_{(u^{t_i}, u^{t_{i+1}}) \sim P_u} \|\alpha[\mathcal{G}^\dagger(u^{t_i}; \theta) - u^{t_{i+1}}] + \beta[\mathcal{T}^{-1} \circ \mathcal{P}_m^{-1} \circ \mathcal{P}_m \circ \mathcal{T}(u^{t_i}) - u^{t_i}]\|_{\mathcal{U}}, \quad (15)$$

331 where $\mathcal{G}^\dagger(u^{t_i}; \theta)$ represents the DyMixOp’s prediction for $u^{t_{i+1}}$, $\|\cdot\|_{\mathcal{U}}$ denotes the norm in the Ba-
 332 nach space $\mathcal{U}(D; \mathbb{R}^{d_u})$, and α, β are the weighted coefficients. The optimization target consists of
 333 the reconstruction and consistency errors. Although the DyMixOp architecture is designed based on
 334 the viewpoint of the evolution of dynamics, it presents a powerful capability to approximate the gen-
 335 eral solution operator mapping parameters to solutions. This will be demonstrated in the following
 336 experiments. In this work, we leverage data pairs of the form $\{[u^{t_{i-k}}, \dots, u^{t_i}], u^{t_{i+1}}\}$ to account
 337 for temporal dependencies. The optimization problem is solved using empirical risk minimization,
 338 approximating the expectation with a finite dataset to effectively train the neural evolutionary oper-
 339 ator.

340 4 RESULTS

341 4.1 EXPERIMENT SETTINGS

344 **Datasets.** We conduct experiments on the following datasets across multiple domains and PDE
 345 types: (i) 1D Kuramoto-Sivashinsky (KS), a one-dimensional parabolic PDE; (ii) 2D Burgers, a two-
 346 dimensional parabolic PDE; (iii) 2D CE-CRP, a two-dimensional hyperbolic PDE; (iv) 2D Darcy
 347 (Li et al., 2020a), a two-dimensional elliptic PDE; (v) 2D Navier-Stokes (NS), a two-dimensional
 348 parabolic PDE; (vi) 3D Brusselator (Bru.), a three-dimensional parabolic PDE; (vii) 3D Shallow
 349 Water (SW) (Cao et al., 2024), a three-dimensional hyperbolic PDE; More details on datasets can
 350 be found in the Appendix.

351 **Baselines.** We compare our method with several well-known models equipped with different trans-
 352 formations: (i) DeepONet (Lu et al., 2021a), a local-transformation-based architecture; (ii) GNOT
 353 (Hao et al., 2023), a global-transformation-based architecture; (iii) FNO (Li et al., 2020a), a LGA-
 354 transformation-based architecture; (iv) PeRCNN (Rao et al., 2023), a concise LLM-transformation-
 355 based architecture; (v) ConvLSTM (Shi et al., 2015), a precise LLM-transformation-based architec-
 356 ture. More details on baselines can be found in the Appendix.

357 **Experiment Details.** For the hyperparameters of the baselines and our methods, we assign different
 358 configurations for all models. By thoroughly exploring a wide range of configurations, we can
 359 comprehensively assess the models’ potential. For fair comparisons, all models are trained for 500
 360 epochs using the learning rate of $1e - 3$ and the AdamW optimizer (Loshchilov & Hutter, 2017)
 361 with 0.97 gamma and 6 step size. StepLR scheduler is utilized to modify the learning rate and a
 362 batch size 128 is used in the training on a single NVIDIA A100 GPU. More details about model
 363 configurations and implementation refer to Appendices

364 **Metrics.** All datasets are normalized in min-max normalization. For all datasets, except the 2D
 365 Darcy dataset, we adopt the mean squared error (MSE) as the reconstruction metric for training and
 366 evaluation. The 2D Darcy dataset employs the relative MSE instead, aiming to address extremely
 367 minimal solutions and prevent gradient vanishing.

369 4.2 MAIN COMPARISON RESULTS

371 The main experimental results for all datasets and methods are shown in Table 1. Based on these
 372 results, we have the following observations.

373 **An Excellent Performance and Generalization on Various PDE Types in the DyMixOp.** Our
 374 DyMixOp model consists of convection-inspired transformations and naturally embeds convection
 375 features into the model, enabling it to effectively capture convection dynamics with satisfactory
 376 performance. This perspective is validated by great gains in the 2D NS and 3D SW datasets, where
 377 these dynamics involve the influence of the convection term. The reduction in prediction error
 exceeds 75% in both cases. It can also be noted in Fig. 2 that the prediction accuracy of the

378

379
380
381
Table 1: For each model, the metric on each dataset is the best one among almost **16** model config-
urations. For each dataset, the optimal result among the models is in **bold**, and the suboptimal result
is underlined.

Model	1D KS	2D Burgers	2D CE-CRP	2D Darcy	2D NS	3D Bru.	3D SW
ConvLSTM	0.8235	0.0326	0.0578	1.9e-6	0.0023	0.4744	7.2e-4
PeRCNN	1.0954	0.0520	0.0947	1.8e-5	0.0311	1.5628	1.5e-3
GNOT	1.7231	0.0316	0.0637	1.7e-7	0.0109	0.2042	6.8e-4
DeepONet	1.7337	0.0402	0.0629	1.7e-6	0.0120	2.6432	1.9e-3
FNO	<u>0.0204</u>	<u>0.0020</u>	<u>0.0239</u>	<u>5.2e-9</u>	<u>0.0013</u>	<u>0.0599</u>	<u>8.3e-5</u>
DyMixOp	0.0139	0.0007	0.0185	3.7e-9	0.0003	0.0538	1.1e-5
Gain	31.9%	65.0%	22.6%	28.8%	76.9%	10.2%	86.7%

390

391

392
393
394
395
396
397
DyMixOp significantly improves as the model size increases. In contrast, other models show only
slight performance improvements with larger sizes. The DeepONet model may even perform worse
with a larger model size compared to a smaller one. Despite being inherently convection-inspired,
the DyMixOp still presents a good generalization to other diffusion-dominated datasets such as the
1D KS and the 2D Darcy dataset, achieving an improvement beyond 25%. Similarly, the DyMixOp
can reach better performances on these datasets as the model size increases.

398

399

400

401

402

403

404

405

406

407

408

409

410

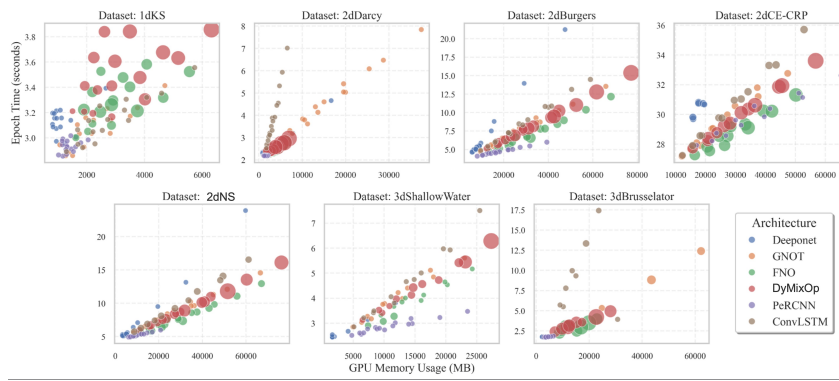
411

412

413

414

415



416

417
418
419
420
421
422
423
424
425
426
427
428
429
430
431
Figure 2: The performance of all model configurations across all datasets is visualized in a plane
defined by training time per epoch and GPU memory usage. The size of each point indicates model
performance, quantified as 1000 divided by the test dataset loss.

450

451

452

453

454

455

456

457

458

459

460

461

462

463

464

465

466

467

468

469

470

471

472

473

474

475

476

477

478

479

480

481

482

483

484

485

486

487

488

489

490

491

492

493

494

495

496

497

498

499

500

501

502

503

504

505

506

507

508

509

510

511

512

513

514

515

516

517

518

519

520

521

522

523

524

525

526

527

528

529

530

531

532

533

534

535

536

537

538

539

540

541

542

543

544

545

546

547

548

549

550

551

552

553

554

555

556

557

558

559

560

561

562

563

564

565

566

567

568

569

570

571

572

573

574

575

576

577

578

579

580

581

582

583

584

585

586

587

588

589

590

591

592

593

594

595

596

597

598

599

600

601

602

603

604

605

606

607

608

609

610

611

612

613

614

615

616

617

618

619

620

621

622

623

624

625

626

627

628

629

630

631

632

633

634

635

636

637

638

639

640

641

642

643

644

645

646

647

648

649

650

651

652

653

654

655

656

657

658

659

660

661

662

663

664

665

666

667

668

669

670

671

672

673

674

675

676

677

678

679

680

681

682

683

684

685

686

687

688

689

690

691

692

693

694

695

696

697

698

699

700

701

702

703

704

705

706

707

708

709

710

711

712

713

714

715

716</

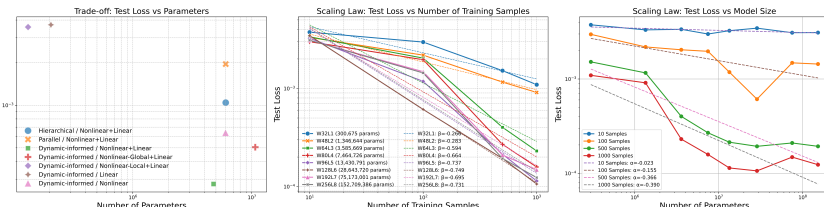
432
433
434
435
436
437
438
439

Figure 3: The illustration of scaling experiments for training samples and model sizes and ablation experiments. 'W' is the channel width and 'L' is the number of layers.

442
443

Ablation Experiments. We conduct ablation studies (Fig. 3) on nonlinear LGM transformations, LGM layers, and the dynamics-informed architecture, using standardized settings (e.g., 96-width channels unless noted). First, replacing the DyMixOp’s nonlinear LGM transformations with purely local or global counterparts degraded performance: local-only failed to capture long-range dependencies, while global-only underperformed despite improvement, confirming that combining both is essential for modeling complex dynamics. Second, isolating linear and nonlinear components in LGM layers showed that linear-only performed poorly due to limited expressiveness, similar to local-only. Nonlinear-only achieved better results but collapsed around 340 epochs from instability, highlighting the need for a balanced integration of both transformation types. Lastly, testing the architecture design revealed that hierarchical stacking caused error accumulation and instability, while parallel stacking was stable but suboptimal. The combined parallel-hierarchical structure, guided by dynamical principles, delivered superior performance. These results emphasize the importance of integrating local and global features, balancing linear and nonlinear transformations, and adopting a hybrid architecture for effective modeling of complex dynamical systems.

450
451
452
453
454
455
456
457
458
459
460
461
462
463
464
465

Scaling Experiments. We adapt the task to non-autoregressive prediction to test a range of model sizes on a single NVIDIA A100 GPU. Eight configurations were examined, from W32L1 (0.3M parameters) to W256L8 (152.7M parameters), across data amounts of 10, 100, 500, and 1000 samples. Performance improved with more data across all model sizes, with larger models (e.g., W128L6) needing substantial data to optimize learning. Performance gains saturated around W128L6, particularly under data-rich regimes, highlighting the benefits of scaling. Spanning three orders of magnitude in size and data, these trends suggest further scaling could yield greater gains, affirming DyMixOp’s potential for complex dynamical systems.

466
467

5 CONCLUSION

468
469
470
471
472
473
474
475
476
477
478
479
480
481
482
483

In this work, we propose **DyMixOp**, a principled neural operator framework that draws inspiration from complex dynamical systems to guide the architecture design for solving PDEs. Unlike prior approaches that often rely on heuristic or architecture-driven construction, our method is grounded in dynamical system theory, offering both theoretical rigor and empirical strength. The main contributions are summarized as follows: **(i) Theory-guided operator modeling:** We leverage **inertial manifold theory** to reduce infinite-dimensional nonlinear PDE dynamics into a finite-dimensional latent space, preserving essential nonlinear interactions. This dimensionality reduction offers a structured foundation for neural operator design with better physical interpretability and efficiency. **(ii) Convection-inspired Local-Global-Mixing (LGM) transformation:** Motivated by the local-global structure of convection terms in turbulence, we introduce a novel transformation that explicitly captures both local features and global interactions through element-wise mixing of local and global kernels. This mitigates spectral bias and enhances the model’s expressiveness across scales. **(iii) Dynamics-informed architecture:** We construct a multi-layer architecture that mirrors the temporal evolution of dynamical systems in a hybrid variant. **(iv) Unified framework for complex PDEs:** By integrating these insights, DyMixOp delivers state-of-the-art performance across a range of PDE benchmarks, including convection-, diffusion-, and mixed-type equations.

484
485

This work demonstrates that **embedding physical and dynamical priors into neural operator design** is not only feasible but also impactful, pointing toward a more systematic path for developing generalizable and efficient neural solvers for complex PDE systems.

486 REFERENCES
487

488 Dzmitry Bahdanau. Neural machine translation by jointly learning to align and translate. *arXiv*
489 *preprint arXiv:1409.0473*, 2014.

490 Kaifeng Bi, Lingxi Xie, Hengheng Zhang, Xin Chen, Xiaotao Gu, and Qi Tian. Accurate medium-
491 range global weather forecasting with 3d neural networks. *Nature*, 619(7970):533–538, 2023.

492 Bernd Blasius, Amit Huppert, and Lewi Stone. Complex dynamics and phase synchronization in
493 spatially extended ecological systems. *Nature*, 399(6734):354–359, 1999.

494 Michael Breakspear. Dynamic models of large-scale brain activity. *Nature neuroscience*, 20(3):
495 340–352, 2017.

496 Steven L Brunton, Marko Budišić, Eurika Kaiser, and J Nathan Kutz. Modern koopman theory for
497 dynamical systems. *SIAM Review*, 2022.

498 Qianying Cao, Somdatta Goswami, and George Em Karniadakis. Laplace neural operator for solving
499 differential equations. *Nature Machine Intelligence*, 6(6):631–640, 2024.

500 Shuhao Cao. Choose a transformer: Fourier or galerkin. *Advances in neural information processing*
501 *systems*, 34:24924–24940, 2021.

502 Mattia Cenedese, Joar Axås, Bastian Bäuerlein, Kerstin Avila, and George Haller. Data-driven
503 modeling and prediction of non-linearizable dynamics via spectral submanifolds. *Nature commu-*
504 *nications*, 13(1):872, 2022.

505 Ricky TQ Chen, Yulia Rubanova, Jesse Bettencourt, and David K Duvenaud. Neural ordinary
506 differential equations. *Advances in neural information processing systems*, 31, 2018.

507 John E Dennis Jr and Robert B Schnabel. *Numerical methods for unconstrained optimization and*
508 *nonlinear equations*. SIAM, 1996.

509 Ciprian Foias, George R Sell, and Roger Temam. Inertial manifolds for nonlinear evolutionary
510 equations. *Journal of differential equations*, 73(2):309–353, 1988.

511 Han Gao, Luning Sun, and Jian-Xun Wang. Phygeonet: Physics-informed geometry-adaptive convo-
512 *lutional neural networks for solving parameterized steady-state pdes on irregular domain. Journal*
513 *of Computational Physics*, 428:110079, 2021.

514 Zhongkai Hao, Zhengyi Wang, Hang Su, Chengyang Ying, Yinpeng Dong, Songming Liu,
515 Ze Cheng, Jian Song, and Jun Zhu. Gnot: A general neural operator transformer for operator
516 learning. In *International Conference on Machine Learning*, pp. 12556–12569. PMLR, 2023.

517 Jonathan Ho, Ajay Jain, and Pieter Abbeel. Denoising diffusion probabilistic models. *Advances in*
518 *neural information processing systems*, 33:6840–6851, 2020.

519 John R Howell, M Pinar Mengüç, Kyle Daun, and Robert Siegel. *Thermal radiation heat transfer*.
520 CRC press, 2020.

521 Frank Jensen. *Introduction to computational chemistry*. John wiley & sons, 2017.

522 Michael I Jordan and Tom M Mitchell. Machine learning: Trends, perspectives, and prospects.
523 *Science*, 349(6245):255–260, 2015.

524 George Em Karniadakis, Ioannis G Kevrekidis, Lu Lu, Paris Perdikaris, Sifan Wang, and Liu Yang.
525 Physics-informed machine learning. *Nature Reviews Physics*, 3(6):422–440, 2021.

526 Hyojin Kim, Junhyuk Kim, Sungjin Won, and Changhoon Lee. Unsupervised deep learning for
527 super-resolution reconstruction of turbulence. *Journal of Fluid Mechanics*, 910:A29, 2021.

528 Jiyeon Kim, Junhyuk Kim, and Changhoon Lee. Prediction and control of two-dimensional decaying
529 turbulence using generative adversarial networks. *Journal of Fluid Mechanics*, 981:A19, 2024.

540 Nikola Kovachki, Zongyi Li, Burigede Liu, Kamyar Azizzadenesheli, Kaushik Bhattacharya, An-
 541 drew Stuart, and Anima Anandkumar. Neural operator: Learning maps between function spaces
 542 with applications to pdes. *Journal of Machine Learning Research*, 24(89):1–97, 2023.

543

544 Isaac E Lagaris, Aristidis Likas, and Dimitrios I Fotiadis. Artificial neural networks for solving
 545 ordinary and partial differential equations. *IEEE transactions on neural networks*, 9(5):987–1000,
 546 1998.

547 Remi Lam, Alvaro Sanchez-Gonzalez, Matthew Willson, Peter Wirsberger, Meire Fortunato, Fer-
 548 ran Alet, Suman Ravuri, Timo Ewalds, Zach Eaton-Rosen, Weihua Hu, et al. Learning skillful
 549 medium-range global weather forecasting. *Science*, pp. eadi2336, 2023.

550

551 Yann LeCun, Yoshua Bengio, and Geoffrey Hinton. Deep learning. *nature*, 521(7553):436–444,
 552 2015.

553

554 Zijie Li, Kazem Meidani, and Amir Barati Farimani. Transformer for partial differential equations’
 555 operator learning. *arXiv preprint arXiv:2205.13671*, 2022.

556

557 Zongyi Li, Nikola Kovachki, Kamyar Azizzadenesheli, Burigede Liu, Kaushik Bhattacharya, An-
 558 drew Stuart, and Anima Anandkumar. Fourier neural operator for parametric partial differential
 559 equations. *arXiv preprint arXiv:2010.08895*, 2020a.

560

561 Zongyi Li, Nikola Kovachki, Kamyar Azizzadenesheli, Burigede Liu, Kaushik Bhattacharya, An-
 562 drew Stuart, and Anima Anandkumar. Neural operator: Graph kernel network for partial differ-
 563 ential equations. *arXiv preprint arXiv:2003.03485*, 2020b.

564

565 Björn List, Li-Wei Chen, and Nils Thuerey. Learned turbulence modelling with differentiable fluid
 566 solvers: physics-based loss functions and optimisation horizons. *Journal of Fluid Mechanics*,
 567 949:A25, 2022.

568

569 Zichao Long, Yiping Lu, Xianzhong Ma, and Bin Dong. Pde-net: Learning pdes from data. In
 570 *International conference on machine learning*, pp. 3208–3216. PMLR, 2018.

571

572 Ilya Loshchilov and Frank Hutter. Decoupled weight decay regularization. *arXiv preprint
 573 arXiv:1711.05101*, 2017.

574

575 Lu Lu, Pengzhan Jin, Guofei Pang, Zhongqiang Zhang, and George Em Karniadakis. Learning
 576 nonlinear operators via deepnet based on the universal approximation theorem of operators.
 577 *Nature machine intelligence*, 3(3):218–229, 2021a.

578

579 Lu Lu, Raphael Pestourie, Wenjie Yao, Zhicheng Wang, Francesc Verdugo, and Steven G Johnson.
 580 Physics-informed neural networks with hard constraints for inverse design. *SIAM Journal on
 581 Scientific Computing*, 43(6):B1105–B1132, 2021b.

582

583 Volodymyr Mnih, Koray Kavukcuoglu, David Silver, Andrei A Rusu, Joel Veness, Marc G Belle-
 584 mare, Alex Graves, Martin Riedmiller, Andreas K Fidjeland, Georg Ostrovski, et al. Human-level
 585 control through deep reinforcement learning. *nature*, 518(7540):529–533, 2015.

586

587 Parviz Moin and Krishnan Mahesh. Direct numerical simulation: a tool in turbulence research.
 588 *Annual review of fluid mechanics*, 30(1):539–578, 1998.

589

590 Siddhartha Mukherjee, Rahul K Singh, Martin James, and Samriddhi Sankar Ray. Intermittency,
 591 fluctuations and maximal chaos in an emergent universal state of active turbulence. *Nature
 592 Physics*, pp. 1–7, 2023.

593

594 Guofei Pang, Lu Lu, and George Em Karniadakis. fpinns: Fractional physics-informed neural
 595 networks. *SIAM Journal on Scientific Computing*, 41(4):A2603–A2626, 2019.

596

597 Jiagang Qu, Weihua Cai, and Yijun Zhao. Learning time-dependent pdes with a linear and nonlinear
 598 separate convolutional neural network. *Journal of Computational Physics*, 453:110928, 2022.

599

600 Maziar Raissi, Paris Perdikaris, and George E Karniadakis. Physics-informed neural networks: A
 601 deep learning framework for solving forward and inverse problems involving nonlinear partial
 602 differential equations. *Journal of Computational physics*, 378:686–707, 2019.

594 Chengping Rao, Pu Ren, Qi Wang, Oral Buyukozturk, Hao Sun, and Yang Liu. Encoding physics
 595 to learn reaction–diffusion processes. *Nature Machine Intelligence*, 5(7):765–779, 2023.
 596

597 Dennis C Rapaport. *The art of molecular dynamics simulation*. Cambridge university press, 2004.
 598

599 Xingjian Shi, Zhourong Chen, Hao Wang, Dit-Yan Yeung, Wai-Kin Wong, and Wang-chun Woo.
 600 Convolutional lstm network: A machine learning approach for precipitation nowcasting. *Ad-*
 601 *vances in neural information processing systems*, 28, 2015.

602 Karen Simonyan and Andrew Zisserman. Very deep convolutional networks for large-scale image
 603 recognition. *arXiv preprint arXiv:1409.1556*, 2014.

604 Gordon D Smith. *Numerical solution of partial differential equations: finite difference methods*.
 605 Oxford university press, 1985.
 606

607 S Succi. *The Lattice Boltzmann Equation for Fluid Dynamics and Beyond*. Oxford University Press,
 608 2001.

609 Lloyd N Trefethen. *Spectral methods in MATLAB*. SIAM, 2000.
 610

611 Tapas Tripura and Souvik Chakraborty. Wavelet neural operator: a neural operator for parametric
 612 partial differential equations. *arXiv preprint arXiv:2205.02191*, 2022.

613 A Vaswani. Attention is all you need. *Advances in Neural Information Processing Systems*, 2017.
 614

615 Henk Kaarle Versteeg. *An introduction to computational fluid dynamics the finite volume method*,
 616 2/E. Pearson Education India, 2007.

617 Oriol Vinyals, Igor Babuschkin, Wojciech M Czarnecki, Michaël Mathieu, Andrew Dudzik, Juny-
 618 oung Chung, David H Choi, Richard Powell, Timo Ewalds, Petko Georgiev, et al. Grandmaster
 619 level in starcraft ii using multi-agent reinforcement learning. *nature*, 575(7782):350–354, 2019.
 620

621 Anqing Xuan and Lian Shen. Reconstruction of three-dimensional turbulent flow structures using
 622 surface measurements for free-surface flows based on a convolutional neural network. *Journal of*
 623 *Fluid Mechanics*, 959:A34, 2023.

624 OC Zienkiewicz. The finite element method in engineering science, 1971.
 625

626

627

628

629

630

631

632

633

634

635

636

637

638

639

640

641

642

643

644

645

646

647